Catalysis Science & Technology

ROYAL SOCIETY OF CHEMISTRY

PAPER

View Article Online
View Journal | View Issue



Cite this: *Catal. Sci. Technol.*, 2025, 15, 3837

# Design, testing and characterization of noble-metal catalysts for the heat-release reaction of a molecular solar thermal energy storage isomer pair†

Benjamin Rollins,*[a] Alberto Gimenez-Gomez,[b] Andrew M. Steele,[a] Helen Hölzel,[c] Rebecca J. Salthouse,[c] Kevin Moreno,[c] Kasper Moth-Poulsen,[cde] Ignacio Funes-Ardoiz *[b] and Diego Sampedro *[b]

MOlecular Solar Thermal systems (MOST) are a promising technology to store solar energy in chemical bonds. The heat release from the charged isomers requires an efficient catalysed reaction to deliver its energy on demand. Herein, a series of heterogeneous catalysts featuring varied metal centres and supports was synthesised and evaluated for the thermal back-conversion reaction of one of the most advanced MOST systems, based on the norbornadiene/quadricyclane photoswitch pair. The catalysts were characterised to understand the effects that influence performance. Two key findings were made. Firstly, the best performing catalysts were those where the metal centres were in a metallic state as opposed to being oxidized. Some metals oxidise more readily on alumina than on activated carbon, and therefore, for these metals, the choice of support has a significant effect. Secondly, catalysts with very low loading had disproportionately high activity compared with higher-loading catalysts. This seems to be due to the presence of highly active and highly dispersed particles at low loading, which are much more active than the larger particles that readily form at higher loadings.

Received 24th March 2025,
Accepted 7th May 2025

DOI: 10.1039/d5cy00366k

rsc.li/catalysis



## Introduction

The transition towards renewable and sustainable energy sources, particularly solar energy, requires efficient solutions to address their inherent intermittency. Solar irradiation is most abundant in the summer months, whereas typical domestic energy demands peak in the winter. In order to ensure that solar energy can be widely used, it must be stored for more than six months with minimal losses and minimal costs. Furthermore, the use of rare or harmful materials must be minimized.

A number of technologies have been developed to store thermal energy. This energy can be stored as sensible heat, latent heat, or thermochemical heat, with each having its associated advantages and disadvantages.[1,2] Thermochemical heat storage, in particular, is associated with high energy storage densities and minimal energy loss, but is often complex and expensive.[3] There have been a number of different studies of different technologies and approaches to integrating solar thermal energy storage into domestic and industrial heating, but so far, with minimal success.[4–9]

Molecular solar thermal (MOST) energy storage systems are a type of thermochemical storage involving individual molecules that undergo photoisomerization to a higher energy metastable state when exposed to solar irradiation. The isomerization can be reverted under either thermal or catalytic activation. There is a range of different molecular systems that have been identified[10,11] but one of the most promising candidates is the norbornadiene/quadricyclane (NBD/QC) isomer pair. NBD has been studied for some years primarily for its use in heat storage as well as in conjunction with thermoelectric generators for electricity production[12,13] and as part of hybrid devices[14–16] or in logic systems.[17] NBD and its derivatives undergo an intramolecular [2 + 2] cycloaddition when exposed to ultraviolet light, forming quadricyclane and its derivatives. The absorption spectrum of NBD, and the kinetics and thermodynamics of the reverse reaction from QC to NBD can be tuned by modifying the functional groups at the 2 and 3 positions.[11,18,19] While many NBD derivatives can be converted to QC with solar irradiation

[a] *Johnson Matthey Technology Centre, Blount's Court Road, Sonning Common, RG4 9NH, UK. E-mail: Benjamin.rollins@matthey.com*
[b] *Department of Chemistry, Instituto de Investigación Química de la Universidad de La Rioja (IQUR), Universidad de La Rioja, Madre de Dios 53, 26006 Logroño, Spain. E-mail: Ignacio.funesa@unirioja.es, diego.sampedro@unirioja.es*
[c] *Department of Chemical Engineering, Universitat Politècnica de Catalunya, EEBE Eduard Maristany, 10-14 08019 Barcelona, Spain*
[d] *Catalan Institution for Research & Advanced Studies, ICREA, Pg. Lluís Companys 23, 08010 Barcelona, Spain*
[e] *The Institute of Materials Science of Barcelona, ICMAB-CSIC, Bellaterra, 08193 Barcelona, Spain*

† Electronic supplementary information (ESI) available. See DOI: https://doi.org/10.1039/d5cy00366k

alone, unsubstituted NBD requires a photosensitizer.[20] The energy barrier of the reverse reaction is correlated with the half-life for uncatalyzed reversion to the NBD isomer and is therefore a key parameter, whilst the portion of the solar spectrum absorbed by the isomer pair will determine the efficiency of the system (Fig. 1a). Storage density is relatively affected by these substitutions. In particular, the isomer pair referred to as NBD1/QC1, shown in Fig. 1, has a remarkably long half-life for reversion from QC1 to NBD1 and absorbs a good portion of the solar spectrum.[21]

Relatively little work has been published in this area on the design, preparation, and characterization of catalysts for the reverse reaction of QC derivatives to their NBD equivalents. This is despite the significant effect that the catalyst can have on the performance of the whole system. A viable catalyst must be: highly active, to maximize peak throughput and heat release in flow systems; stable, to ensure long lifetimes; and heterogeneous, to ensure that the reverse reaction occurs only where desired.

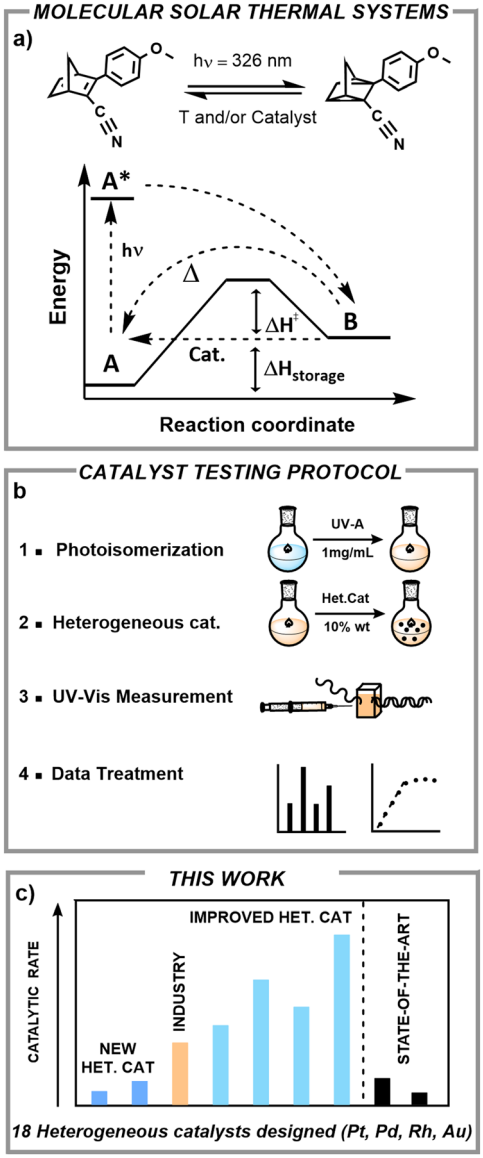


Fig. 1 a) Schematic representation of the MOST system studied in this manuscript. b) Protocol developed to test heterogeneous catalysts. c) This work.

Initial research that discussed catalysts focused mainly on homogeneous catalysis using metal complexes, including porphyrins, phthalocyanines, and other complexes of transition metals, often cobalt.[12,21–25]

Platinum-group-metal (PGM) catalysts have also received some attention.[26] In particular, Pt surfaces have been shown to be effective for the conversion of monolayers of QC to NBD, with the effect of different surface sites being investigated.[27] It was shown that QC rapidly converts to NBD upon contact with the (111) surfaces of metals such as Pt and Ni[28] before eventually decomposing. Decomposition products are difficult to determine, but on Ni, the removal of the bridgehead carbon of NBD leading to the formation of benzene was proposed. It is unknown if a similar process would occur for NBD1/QC1 or in solution. In contrast, similar experiments were performed with another NBD/QC derivative pair on Au (111).[29] In this example, the NBD/QC derivatives did not break down on the surface of the metal, instead, they were desorbed entirely at higher temperatures. This seems to be due to a different adsorption geometry. Metal surfaces possess some appealing advantages over transition metal complexes for scalability, such as the ability to physically separate the catalyst and the reaction solution, and therefore, further research into heterogeneous catalysts for this reaction is desirable.

Recently, we have reported a simple but effective screening regime for testing the performance of heterogeneous catalysts for the conversion of QC1 to NBD1 (Fig. 1b).[30] It was demonstrated that this method allowed good differentiation of the performance of different catalysts and also that while most of the tested catalysts were based on Pt/C, the loading of metal, the exact supporting carbon and the preparation method all had a profound effect on the performance. It is well known that there are significant complexities to the performance of a heterogeneous catalyst besides the active metal of choice. This can include the support material, including modifications to the structure and surface groups of the support, as well as the type of heat treatment used, if any, and the metal precursor used. Amongst others,[31–33] these effects should be investigated systematically.

In this paper, a variety of PGM and Au catalysts, supported on γ-alumina and carbon, are tested for their performance in converting QC1 to NBD1 in different solvents using a method described previously (Fig. 1c).[30] The differences in activity are investigated by a range of characterization techniques and by preparing low-loading analogues to determine the relative activity of different active metal sites.

## Materials and methods

### Catalyst preparation

Eight catalysts were prepared initially. These catalysts were impregnated with Pt, Pd, Rh, or Au on activated carbon or

 

γ-alumina supports. Pt, Pd, and Rh catalysts were impregnated using the nitrate solution of the respective metals. The gold catalysts were impregnated with a suspension of gold(III) acetate. The quantity of the precursor was selected to give the appropriate weight percentage (wt%) of metal after drying and calcination, and the quantity of water was chosen to fill 95% of the support pore volume. The catalysts were then dried in an oven at 105 °C for 8 hours and were calcined for 2 hours under flowing nitrogen at 400 °C with a ramp rate of 10 °C $min^{-1}$. The exception to this was the gold catalysts, which were calcined at 200 °C due to the propensity of gold nanoparticles to sinter. Subsequently, eight further catalysts were made in the same way but at a loading of 0.1 wt%.

### Characterization

The Brunauer–Emmett–Teller (BET) surface areas for each of the catalysts were measured using a Micromeritics TriStar II Plus™ instrument. The measured pressure and quantity of gas adsorbed were normalized to standard temperature and pressure.

Transmission electron microscopy (TEM) images were collected using a JEOL 2800™ instrument with a primary electron energy of 200 keV and a point resolution of 1 Å.

The actual loadings of the catalysts, as opposed to theoretical loadings, were determined by inductively coupled plasma-optical emission spectroscopy (ICP-OES). An Agilent ICP-OES 5110 Series™ instrument with a humidifier was used. Samples were prepared by microwave-assisted digestion in inverse aqua regia.

X-ray diffraction (XRD) was used to determine the phases present in each catalyst sample. The measurements were made using a Bruker D8 ADVANCE DAVINCI.DESIGN™ instrument with Cu Kα radiation and Bragg Brentano geometry.

The oxidation states of the metals present in the catalysts were determined by X-ray photoelectron spectroscopy (XPS). The study was carried out with a Thermo Nexsa™. The radiation used was monochromatized aluminium Kα radiation with a 650 μm spot size. Charge compensation was provided by the in-lens electron flood gun at a 2 eV setting and the "401" unit for "zero energy" argon ions.

Reduction profiles of the catalysts were determined by temperature programmed reduction using a Micromeritics AutoChem II 2920™ instrument. The catalysts were first cooled to −40 °C using liquid nitrogen under argon and were then heated at 10 °C $min^{-1}$ to 200 °C in flowing gas (10% hydrogen in argon). Water was collected from the product gas feed using a cold trap, and the dry gas was measured using a thermal conductivity detector (TCD).

### Catalyst testing

Two different UV-vis methods were employed to characterize the catalyst used in this study. First, a previously reported method was applied, requiring only a minimal amount of material, both the catalyst and substrate (NBD1). This method has been used in previous studies to evaluate state-of-the-art commercial catalysts, providing a reliable basis for comparison. By adopting this approach, we ensured the reproducibility of the results and established a direct reference for assessing the new catalysts. Subsequently, a second method was implemented to accommodate higher concentrations. This approach allowed us to investigate the effect of concentration on the performance of the new catalysts, offering additional insights under extended conditions.

**Method 1.** Following the protocol recently reported by our group,[30] a 10 mL vial containing 1 mg $mL^{-1}$ ($4.29 \times 10^{-3}$ M) NBD1 solution was irradiated in a photoreactor (setup in Fig. S1†). The solvents used were toluene and Duratherm-HTO22, a commercial alkane-based heat transfer fluid.

The corresponding amount of catalyst required to achieve a 10 wt% ratio (1.0 ± 0.1 mg) was added to a vial containing a stirring bar, followed by the freshly photoconverted QC1 solution.

Periodic UV-vis measurements were performed by sampling, diluting with toluene, and filtering the mixture. Notably, Duratherm samples were also diluted into toluene, as the presence of aromatic compounds in Duratherm could otherwise interfere with measurements in the ultraviolet region of the UV-vis spectrum. To prevent artifacts from fine particles generated during stirring, samples were filtered using 0.44 μm filters. Finally, they were diluted to fall within the linear range of a previously established calibration curve, which provided a linear fit in the absorbance range of the UV-vis detector (*ca.* $10^{-4}$ M).

**Method 2.** NBD1 was dissolved in toluene at a concentration of 3.3 mg $mL^{-1}$ ($1.48 \times 10^{-2}$ mol $dm^{-3}$) to make up a standard testing solution. An equivalent solution was made up using Isopar paraffin as the solvent. This solvent was chosen due to its low flammability and toxicity compared with toluene, whereas toluene was used due to its relevance to earlier tests. The solutions were exposed to UV radiation from a lamp, within a UV protective screen, under stirring for four hours (Fig. S1†). This ensured the total conversion of NBD1 to the corresponding QC1 (Fig. S4†).

A small amount of catalyst was added to a beaker with a stirrer bar. The amount of catalyst used depended on the experiment; unless otherwise specified, it was 5 mg. 3 ml of QC1 solution was added to the catalyst, and the mixture was stirred vigorously for one hour at room temperature. After this time, the mixture was filtered using a syringe filter to remove the catalyst. 40 μL of reaction solution was taken and diluted with 3.6 ml of toluene to provide a solution with an absorbance in the correct range for UV-vis analysis (Fig. S5†).

The product solutions were analysed by UV-vis using PMMA cuvettes. Reference measurements of pure NBD1 solution and fully isomerized QC1 solution were used to give examples of absorbance at 100% and 0% conversion, respectively. NBD1 absorbs strongly at 325 nm, whereas QC1 does not absorb at this wavelength, instead, it absorbs below

300 nm. Further, it was found that there is a linear relationship between the NBD1 concentration and absorbance intensity, and no significant by-products are created during back-conversion. Therefore, the peak at 325 nm could be used to measure the concentration of NBD1 and hence the extent of back-conversion to NBD1. The UV-vis spectra of a NBD1 solution, a QC1 solution, and a 1 : 1 mixed solution of NBD1 and QC1 are shown in Fig. S12.† The calibration curve made from these results is shown in Fig. S13.†

# Results

### Catalyst characterization

The 16 catalysts were characterized by $N_2$ physisorption, transmission electron microscopy, and ICP-OES in order to determine the BET surface area, average metal particle size, and actual metal loading of the catalysts. The results are shown in Table 1. It can be seen that the BET surface area strongly depends on the support, as expected. Activated carbon has a surface area around ten times higher than the alumina support. There is some variation between different carbon-supported catalysts and between different alumina-supported catalysts, but this is generally a comparatively small variation. The exception to this is the 0.1 wt% Au/C catalyst, which has a much lower surface area than the other carbon-supported catalysts. The $N_2$ physisorption isotherms for all the catalysts are shown in Fig. S14 and S15.† The shape of the isotherms (type I for carbon-based catalysts and type IV for alumina-based catalysts) indicates that the carbon-supported catalysts have primarily microporous structures, whereas the pores of the alumina-supported catalysts are larger. This fits well with the observation that the alumina support has a lower surface area.

The metal particles are generally in the size range of several nanometres in diameter with a standard deviation of a few nanometres. The Rh catalysts have significantly smaller particles than the other catalysts, with average particle diameters below 2 nm. Average particle diameters could not be determined for the 0.1 wt% $Pt/Al_2O_3$, $Pd/Al_2O_3$, and $Rh/Al_2O_3$ catalysts due to the small number of particles that could be discerned. For this reason, the particle sizes of 0.1 wt% Au/C, $Au/Al_2O_3$, and Rh/C are also given only tentatively.

### 5 wt% catalysts

The TEM images for the 5 wt% catalysts are shown in Fig. S16.† Particle sizes are presented in Table 1. Pt/C has large, clearly defined Pt particles, including clusters, while the Pt particles on $Pt/Al_2O_3$ are generally somewhat smaller. Pd particles in Pd/C are around the same size as Pt in Pt/C at 7.42 ± 2.33 nm. $Pd/Al_2O_3$ has the largest particles observed. Both rhodium catalysts have much smaller particles than any other catalyst at 1.78 ± 0.36 nm and 1.03 ± 0.37 nm. The gold catalysts have relatively small particles, though larger than the rhodium catalysts. Particle size distributions are shown in Fig. S17.† Higher resolution TEM later confirmed that Pt/C, Pd/C, and Rh/C all have some single atom sites, whereas Au/C and the alumina-supported catalysts do not.

The XRD spectra for the carbon-supported catalysts are shown in Fig. 2. The carbon itself is amorphous. The Rh/C catalyst (purple trace) shows no peaks associated with Rh phases. Assay results confirmed that Rh is present in the sample at 5.03 wt%, and TEM shows small Rh particles with an average diameter of 1.8 nm. Therefore, it is likely that the Rh particles are invisible to XRD due to their small size. Pt/C (green trace) shows strong peaks at $2\Theta$ values of approximately 40, 46, 67, 81, 86, 103, 117, and 123, corresponding to metallic platinum. Pd/C (red trace) shows much weaker peaks that correspond to palladium metal. Finally, Au/C (blue trace) shows very strong peaks corresponding to metallic gold. Each catalyst shows some peaks that could not be assigned. Therefore, Au/C and Pt/C have highly crystalline metal centres, whereas Pd/C has less

Table 1 Characterization data for the noble metal catalysts

| Metal/support | BET surface area ($m^2\ g^{-1}$) | Average metal particle size (nm) | Catalyst loading (wt%) real/theor. |
|---|---|---|---|
| Pt/C | 1037 | 7.7 ± 3.6 | 4.55 (5) |
| Pt/C | 1411 | 5.2 ± 3.7 | 0.12 (0.1) |
| $Pt/Al_2O_3$ | 83 | 5.3 ± 2.7 | 5.27 (5) |
| $Pt/Al_2O_3$ | 103 | N.M. | 0.11 (0.1) |
| Pd/C | 1214 | 7.4 ± 2.3 | 5.27 (5) |
| Pd/C | 1449 | 6.8 ± 2.5 | 0.10 (0.1) |
| $Pd/Al_2O_3$ | 101 | 8.8 ± 2.9 | 5.16 (5) |
| $Pd/Al_2O_3$ | 106 | N.M | 0.09 (0.1) |
| Rh/C | 1168 | 1.8 ± 0.4 | 5.03 (5) |
| Rh/C | 1315 | 0.4 ± 0.6 | 0.13 (0.1) |
| $Rh/Al_2O_3$ | 107 | 1.0 ± 0.4 | 4.90 (5) |
| $Rh/Al_2O_3$ | 94 | N.M. | 0.10 (0.1) |
| Au/C | 1274 | 6.3 ± 2.5 | 3.75 (5) |
| Au/C | 396 | 8.6 ± 5.4 | 0.12 (0.1) |
| $Au/Al_2O_3$ | 96 | 6.4 ± 3.4 | 5.95 (5) |
| $Au/Al_2O_3$ | 97 | 5.2 ± 2.6 | 0.12 (0.1) |

N.M.: not measurable.

 

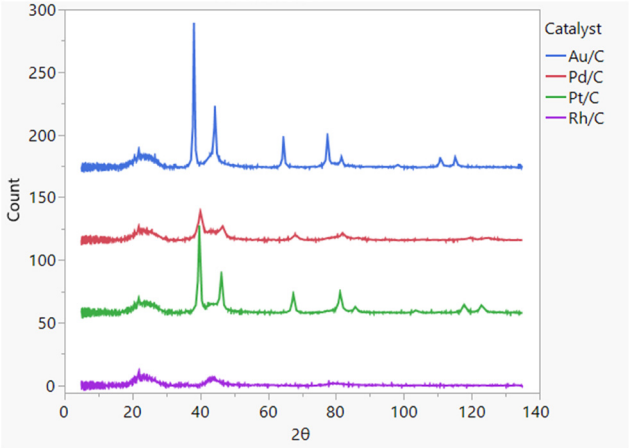


Fig. 2 XRD spectra for the carbon-supported catalysts.

strongly crystalline metal centres, and the Rh in Rh/C is amorphous.

The XRD spectra for the alumina-supported catalysts are shown in Fig. 3, along with that of the γ-alumina support. The alumina support (brown trace) shows characteristic, and fairly broad, peaks at 2$\Theta$ values of approximately 19, 33, 37, 39, 45, 60, 67, 84, and 100. These peaks are present in all of the alumina-supported catalysts, indicating that the general structure of the support has not been changed. Rh/$Al_2O_3$ (purple trace) has the same spectrum as alumina with no Rh-associated peaks. Once again, the presence of Rh in the sample was confirmed by assay at 4.90 wt% loading of Rh, and TEM further demonstrated the presence of small Rh particles. Therefore, like Rh/C, it is likely that the Rh particles are simply too small to be visible to XRD. Pd/$Al_2O_3$ (red trace) has peaks at 2$\Theta$ values of approximately 34, 41, 54, 60, 71, 89, and 100, which correspond to PdO (palladinite). There are no peaks identified as belonging to Pd metal. Therefore, the crystalline Pd in Pd/$Al_2O_3$ is present as the oxide form. Pt/$Al_2O_3$ has peaks at approximately 40, 45, 68, 81, 85, 117, and 122 2$\Theta$. These peaks correspond to metallic platinum. Finally, Au/$Al_2O_3$ has peaks at 2$\Theta$ values of approximately 38, 44, 65, 77, 82, 111, and 115 2$\Theta$. These correspond to metallic gold. Therefore, like the carbon-supported catalysts, the platinum and gold catalysts on alumina have metal in a crystalline, metallic form, and the rhodium catalyst has no rhodium particles large enough to be detected. In contrast, Pd on Pd/$Al_2O_3$ is in its oxide form compared with the metallic form for the carbon-supported equivalent. It is always possible for amorphous phases of any metal to be present, which are invisible to XRD in addition to any detectable phases. All metals are present in the same phases on alumina as on carbon with the exception of palladium, which is present as palladium metal on carbon and palladinite on alumina. It is possible that the lattice oxygen in alumina facilitates the oxidation of the metal, or that carbon supports cause the metal to reduce.

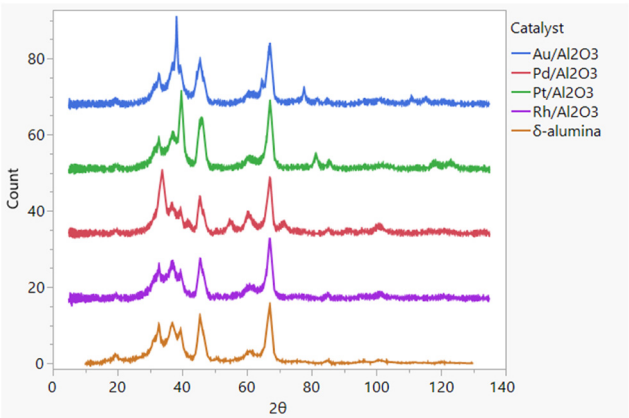


Fig. 3 XRD spectra for the alumina-supported catalysts.

The XPS spectra for these catalysts are shown in Fig. S18.† The Pt/C catalyst displays a doublet peak at 71 eV, which corresponds to metallic platinum. For Pt/$Al_2O_3$, there is an intense Al peak at 74.5 eV. This peak makes it hard to see that there are actually two overlapping peaks between 72 and 71 eV. These correspond to two different Pt [0] environments, although an exact assignment was not possible. There is also possibly some oxidized Pt. These results match the XRD data.

For Pd/C, there is a peak at 335 eV corresponding to Pd [0]. There is also a second, minor peak at 336 eV, which corresponds to PdO. The Pd/$Al_2O_3$ sample, in contrast, also shows a doublet but has a shoulder at a lower binding energy of around 336–335 eV. Here, the main peak corresponds to PdO, and the shoulder is for the Pd [0] species. Therefore, in Pd/C, there is mainly metallic palladium with some palladium oxide, whereas the Pd/$Al_2O_3$ catalyst has mainly Pd oxide with a smaller amount of Pd metal. The XRD data showed only the major species in both cases.

For Rh/C, the baseline of the spectrum is much higher than for Rh/$Al_2O_3$ and also rises towards higher binding energy. This is because the C 1s peak is very close to the Rh peaks and is much more intense. Rh/C has a very complex spectrum, including peaks for oxidized rhodium at 308 and 310 eV. There also appears to be a shoulder at 307 eV corresponding to metallic rhodium. Rh/$Al_2O_3$ shows only oxidized rhodium. These species showed no peaks in the XRD spectra. Presumably, the particles are too small to appear in the XRD.

Au/C and Au/$Al_2O_3$ both show very similar doublet peaks at around 84 eV. These peaks correspond to metallic gold, in good agreement with the XRD data. Au/$Al_2O_3$ also shows a peak at around 75 eV, which corresponds to aluminium. The catalysts were further characterized by temperature programmed reduction (TPR) from −40 °C to 200 °C. The results are shown in Fig. 4 for the alumina and carbon-supported catalysts. From the results for the alumina-supported catalysts, it can be seen that the Pt, Pd, and Rh catalysts all show strong peaks, whereas the gold catalyst has a flat trace. The Pt catalyst has the smallest peak and is centred at the lowest temperature (22 °C), Pd has the tallest

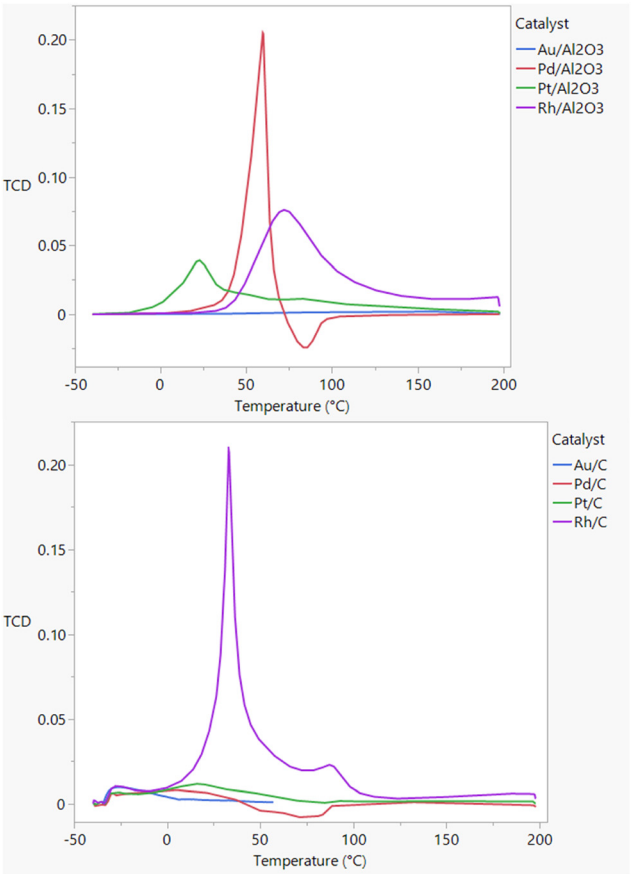


**Fig. 4** TPR profiles for 5 wt% loading alumina (top) and carbon (bottom) supported catalysts.

peak (60 °C), and Rh has the broadest, highest temperature peak (72 °C). The platinum trace also seems to have two small, broad peaks centred at around 46 °C and 81 °C, and the palladium catalyst shows an unexplained negative peak at 85 °C. Amongst these catalysts, the gold and platinum catalysts are the most active in both toluene and paraffin. It is likely that while the Pd and Rh catalysts are significantly oxidized and only reduced at high temperatures, gold is entirely metallic, and platinum is mostly metallic with only a small portion of oxidized character that is more easily reduced than the other metals. This fits with the XRD and XPS data. The additional peaks for Pt/C at 46 °C and 81 °C may indicate the presence of multiple different oxidized platinum phases.

The carbon-supported catalysts show mostly flat traces (with some very small peaks at around −28 °C and, in the case of Pd/C, at 18 °C). The exception is Rh/C, which has a very sharp and intense peak at 33 °C and another smaller peak at 89 °C. The XPS data showed that the metal species of all of these catalysts had a primarily metallic character, which agrees with the TPR data except for Rh, with only a small amount of oxidized Rh in XPS. Therefore, it is unclear why there is such a large peak. All four carbon-supported catalysts are active, and this is likely because they all have at least some metallic character.

### 0.1 wt% catalysts

The TEM images for the 0.1 wt% catalysts are shown in Fig. S19.† As the loading is so low, multiple images were required to calculate the particle size distribution. Even with this approach, some of the catalysts would ideally have benefitted from additional measurements. Of the alumina-supported catalysts, only $Au/Al_2O_3$ had particles that could be measured reliably, whereas all of the carbon-supported catalysts had measurable particles. The particles that could be measured were generally small and well defined, with mean particle sizes between 5 and 9 nm in diameter. Rh/C had a bimodal distribution with many highly dispersed particles, possibly atomically dispersed, and a smaller number of larger particles, around 1–2 nm in diameter. Pt/C and Pd/C also showed the possible presence of atomically dispersed metal particles. It is possible that these small metal sites, where present, help explain the disproportionate activity of 0.1 wt% catalysts compared with 5 wt% catalysts. No conclusions can be drawn about the alumina-supported catalysts as to the presence of atomically dispersed sites due to the poor contrast between the metals and the alumina support.

The XRD images for the carbon-supported catalysts are shown in Fig. S20,† the carbon itself is amorphous with only a few peaks assigned to tridymite. The Rh/C and Pd/C catalysts show no peaks that can be assigned to any phases other than those present in the bare support. Therefore, any metal in these catalysts must be amorphous, finely dispersed, or otherwise not visible to XRD. Pt/C shows very weak peaks for crystalline Pt metal at $2\Theta$ values of 40, 67, and 86. These peaks are hardly visible and appear as slight peaks above the trace of the bare support. Au/C shows somewhat stronger peaks corresponding to metallic gold at $2\Theta$ values of approximately 38 and 64.

The XRD images for the alumina-supported catalysts are shown in Fig. S21,† along with that of the delta-alumina support. None of the catalysts show peaks that are not present for the bare support. Therefore, the metal must be amorphous, finely dispersed, or otherwise invisible to XRD.

These catalysts were also tested by TPR according to the same method as for the 5 wt% catalysts, and the results are shown in Fig. 5. For the alumina-supported catalysts, there are no clearly definable peaks visible. $Pt/Al_2O_3$ and $Rh/Al_2O_3$ have step-change increases in the TCD signals at 43 °C and 111 °C, respectively, although these are very small changes.

Rh/C has a small peak at −26 °C with a shoulder at −17 °C, with additional smaller peaks at 30 °C and 73 °C. Pt/C has a peak at −29 °C with further peaks at −6 °C and 22 °C. Pd/C has peaks at −27 °C, 0 °C, and 30 °C. Au/C has a peak at −26 °C with a shoulder at −16 °C and a smaller peak at 27 °C. Each carbon-supported catalyst, therefore, has multiple oxidized phases, although the majority of the reduction occurs below 0 °C. The low temperature peaks match those present in the equivalent 5 wt% catalysts. It is likely that these matching peaks correspond to the same phases, most likely a highly active phase, as the 0.1 wt% catalysts have disproportionately high activity for their low loading.

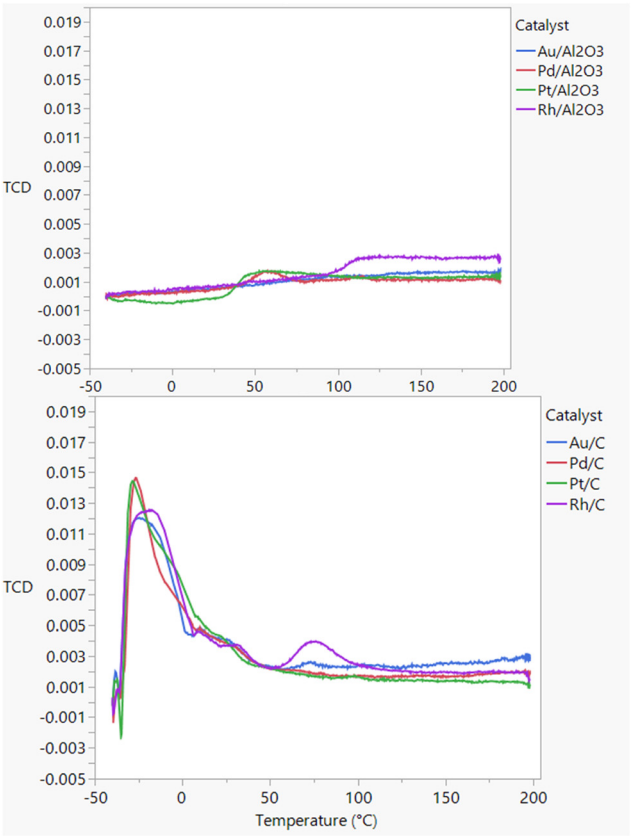


Fig. 5 TPR profiles for 0.1 wt% loading alumina (top) and carbon (bottom) supported catalysts.

### Catalyst testing at low NBD1 concentration (Method 1)

For the catalyst testing at low concentration, four different catalysts were initially evaluated using the previously reported UV-vis method (Method 1, see section 2.2). The selected catalysts consisted of two platinum-based systems ($Pt/Al_2O_3$ and Pt/C) and two gold-based systems ($Au/Al_2O_3$ and Au/C), all with a metal loading of 5 wt%.

The choice of platinum catalysts was particularly motivated by earlier studies,[30] which demonstrated that platinum exhibited superior performance compared to other metals using the same MOST system (NBD1/QC1). Furthermore, a commercially available standard catalyst (Au/NPs < 5 nm) was included in the selection, as it has been tested in similar systems.

Consequently, the composition of these four catalysts was chosen to enable a direct comparison between platinum, in alignment with previous literature reports, and gold, to compare with an industry standard catalyst,[30] justifying the presence of both gold and platinum systems in this first approach.

Following the initial evaluation, the $Pt/Al_2O_3$ catalyst demonstrated outstanding performance in toluene and in Duratherm-HTO22. Based on this observation, additional samples with lower metal loadings (1 wt% and 3 wt%) were synthesized and tested to assess whether the metal concentration played a limiting role in the observed activity

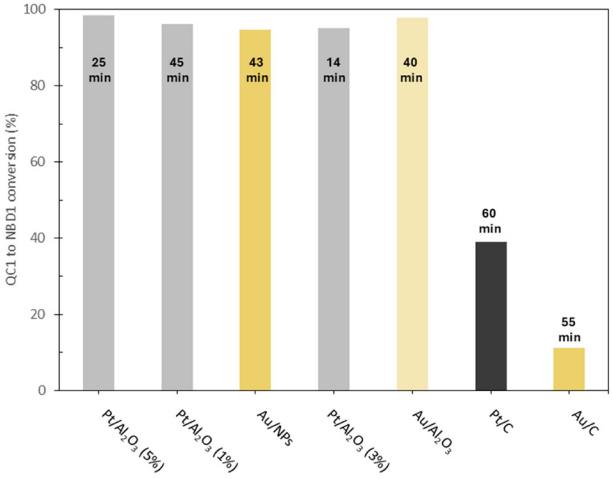


Fig. 6 QC1 back conversion using different catalysts after reaching 60 min or >95% NBD1 in toluene.

only in toluene. These additional experiments provided insights into the influence of metal loading on the catalytic performance and helped establish the optimal balance between efficiency and material usage. For a direct comparison with Method 2, a timeframe of 1 hour was selected to compare the conversions of the different catalysts (Fig. 6 and 7).

As observed, most catalysts achieve >95% conversion within the first hour of catalysis, except those supported on carbon, such as Pt/C and Au/C, which fall short of this benchmark. It is possible that the industry standard, based on gold nanoparticles <5 nm supported on carbon, is functionalized differently, as it performs comparably to the rest of the catalysts.

For the tests conducted in Duratherm-HTO22, only the 5 wt% catalysts were evaluated (excluding the 1 wt% and 3 wt% $Pt/Al_2O_3$ catalysts). In this case, only the 5 wt% $Pt/Al_2O_3$ catalyst reached 80% conversion after one hour. The second-best performer was the industry-standard gold catalyst,

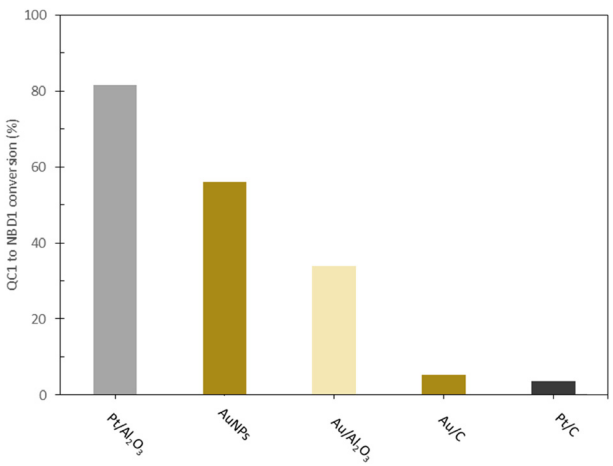


Fig. 7 QC1 back conversion measured in Duratherm-HTO22 after 1 hour with the four 5 wt% catalysts and the industry standard.

though this may be attributed to the size of the nanoparticles. Since its particle size was not directly comparable to the other four catalysts, definitive conclusions cannot be drawn. However, it appeared to have a finer size and exhibited better dispersion. Although this is not the main aim of this study, these results allowed for the assessment of the performance of different solvents in the catalysed back-reaction of QC to NBD.

Using the previously reported method, we enabled a direct comparison with commercial catalysts and existing benchmarks. This approach allowed us to contextualize the results within the broader framework of MOST catalyst development and to further validate the observed trends.

A key advantage of Method 1 is that conversion is measured at different points in time (besides 1 hour); this allows for the determination of the catalytic rate constant ($k_{cat}$), which is a more practical parameter for comparing different catalysts. To ensure a direct comparison with Method 2, the conversion percentage after 1 hour was also measured. However, as some catalysts reached 100% conversion much earlier, we also include Fig. 8 and 9, where the $k_{cat}$ values are presented for a more comprehensive analysis. The rate values were obtained by analysing the linear trend between the evolution of the natural logarithm of the QC1 concentration (ln[QC1]) over time (see Fig. S6–S11†). This approach ensures that $k_{cat}$ can be accurately determined even when complete conversion is achieved, preventing misleading interpretations that could arise from comparing conversion levels at a fixed time point.

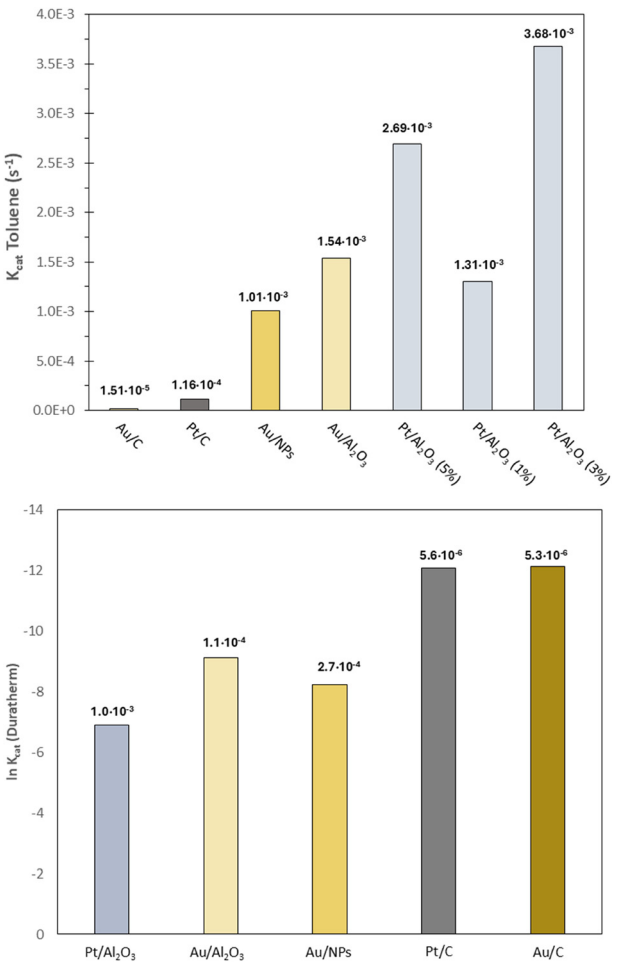


Fig. 8 Top) Catalytic rate constants of the different catalysts measured in toluene by method 1. Indicated values correspond to the $k_{cat}$. Bottom) Logarithmic representation of the rate constants of the different catalysts in Duratherm-HTO22. Indicated values correspond to the $k_{cat}$.

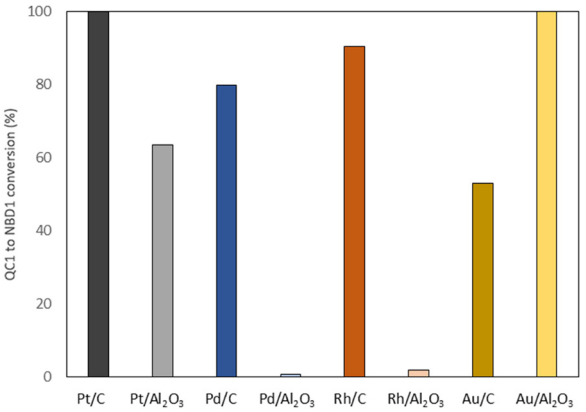


Fig. 9 QC1 back conversion using different catalysts at 5 wt% loading in toluene.

However, when the tests are conducted in a considerably more viscous solvent (Duratherm-HTO22), these differences become even more pronounced. Catalysts supported on carbon exhibit a reduction in activity by 2 to 3 orders of magnitude compared to the most effective alumina-supported catalysts, whether platinum or gold. Surprisingly, in this solvent, the industry standard based on gold nanoparticles attached to a carbon support performs similarly to the $Au/Al_2O_3$.

After an initial assessment, it can be observed that the trends identified in previous studies persist: platinum remains the most effective metal, outperforming even gold.[30] However, the alumina support used in this study proves superior to previously reported carbon-based supports. While it is difficult to confirm whether the formulations are identical, given their commercial nature, the carbon-supported catalysts tested in this study show significant improvement compared to earlier versions, although they still fall short of the performance achieved with alumina-based supports.

After testing at a concentration of 1 mg $mL^{-1}$ for NBD1 and obtaining reasonable $k_{cat}$ values ($\approx 10^{-3}$ $s^{-1}$), the natural next step is to transition to higher NBD1 concentrations. Higher concentrations would increase the capacity of the system for energy storage within the MOST framework. From this point forward, the experiments are conducted following method 2.

## Catalyst testing at high NBD1 concentration (Method 2)

**5 wt% catalysts.** The results for the testing of the 5 wt% catalysts in toluene are given in Fig. 9. It can be seen that for the

catalysts supported on carbon, all of the catalysts are active, but there is a trend of activity in the following order: Pt > Rh > Pd > Au. The platinum-based catalyst has a conversion of almost 100%, and the gold-based catalyst has a conversion of 52.8%. On the other hand, for the alumina-based catalysts, the platinum and gold-based catalysts are very active. The platinum-based catalyst has a conversion of 63.4%, and the gold-based catalyst has a conversion of almost 100%. The rhodium- and palladium-based catalysts have very low activity. It is interesting to note that the gold-based catalyst is the least active of the carbon-supported catalysts but is the most active of the alumina-based catalysts.

The results for the testing in Duratherm-HTO22 are given in Fig. 10. For the carbon supported catalysts, conversion in paraffin is significantly lower except for Au/C which is only slightly lower. Furthermore, the trend of activity, which in toluene was Pt > Rh > Pd > Au, becomes Pt > Au > Pd > Rh in paraffin. The highest conversion achieved for a carbon supported catalyst was 53.6% for Pt/C whilst the lowest was 24.4% for Rh/C. For alumina supported catalysts, the results are more variable. The highly performing alumina supported catalysts have higher conversion than any carbon-supported catalysts, whereas the poorly performing alumina catalysts are worse than any carbon catalyst.

The activity order for the alumina supported catalysts is Pt > Au ≫ Rh > Pd. $Pt/Al_2O_3$ has a conversion of 93.9%, whereas $Pd/Al_2O_3$ has only 3.4% conversion. It is interesting to note that the two alumina catalysts that performed particularly poorly in paraffin were the same as those that performed poorly in toluene. Three catalysts performed better in paraffin than in toluene, these were $Pt/Al_2O_3$, $Rh/Al_2O_3$, and $Pd/Al_2O_3$. $Au/Al_2O_3$ performed better in toluene than in paraffin but was still the second most active catalyst in paraffin.

**0.1 wt% catalysts.** The XPS and TPR profiles for several of the catalysts seen previously implied the presence of multiple metal-containing phases in those catalysts. In order to investigate this, a set of catalysts was prepared identically to those described above but with 0.1 wt% loading instead of 5 wt%. The BET surface areas, average metal particle sizes, and actual loadings for these catalysts are described in Table 1. It was thought that a low loading of metal would be likely to favour high dispersion. If this were found to be the case, then the activity of these low loading catalysts would provide information on the relative activities of small, highly dispersed particles compared with larger particles, which are more likely to form in the 5 wt% catalysts. This would give information about the kind of metal sites that are most active for the reaction.

The 0.1 wt% catalysts were tested according to the standard procedure, but with 25 mg of catalyst instead of 5 mg. This was done to increase the amount of metal present in the reaction and to better compare with the 5 wt% catalysts. The mass of metal could not be matched as the amount of catalyst required would produce a slurry that would not have been stirred or filtered well.

The results for the testing in toluene are given in Fig. 11. In the case of the catalysts supported on carbon, all of the catalysts are active, but there is a trend of activity in the following order: Pt > Pd > Rh > Au. This is similar to the trend for the 5 wt% catalysts except that Rh and Pd are switched. The platinum-based catalyst has a conversion of about 100%, and the gold-based catalyst has a conversion of 65%.

On the other hand, for the alumina-based catalysts, only the platinum and gold-based catalysts are active. This is the same result achieved for the 5 wt% catalysts. The platinum-based catalyst has a conversion of about 100%, and the gold-based catalyst has a conversion of 54%. The rhodium- and palladium-based catalysts have a conversion below 1%.

It is interesting to note that the gold-based catalyst is the least active of the carbon-supported catalysts but is the second-most active of the alumina-based catalysts. The broad trends for these catalysts are the same as those at 5 wt% loading. What is interesting to note is that these reactions contained a tenth of the amount of metal, spread over 5 times the support mass, and yet similar conversions were achieved. In fact, the Pt/C catalyst achieved a higher conversion here than for the 5 wt% catalyst. Therefore, it may be that the metal sites favoured by low loading

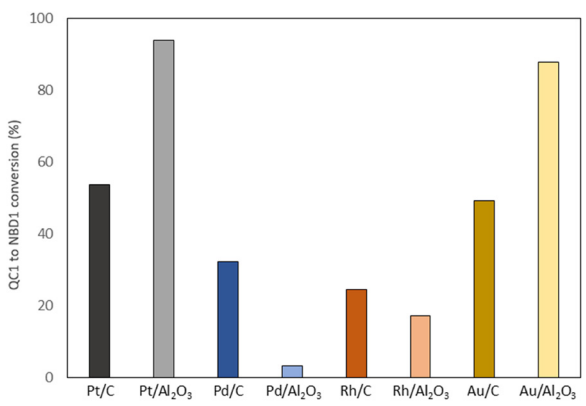


Fig. 10 QC1 back conversion using different catalysts at 5 wt% loading in Duratherm.

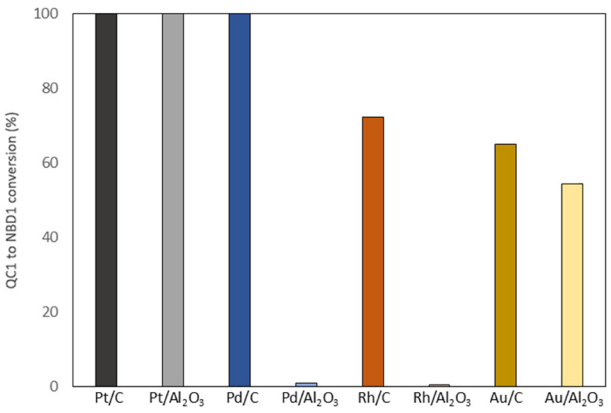


Fig. 11 QC1 back conversion using different catalysts at 0.1 wt% loading in toluene.

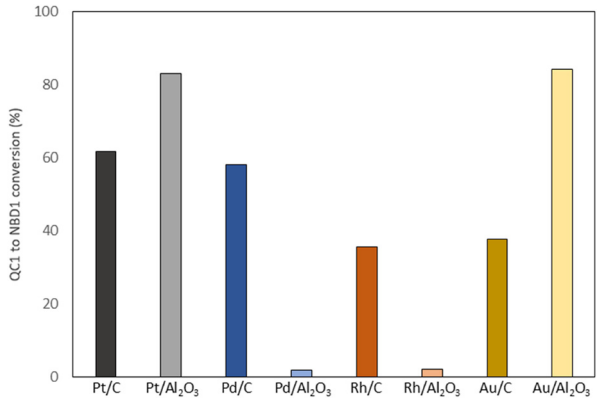


Fig. 12 QC1 back conversion using different catalysts at 0.1 wt% loading in Duratherm.

(potentially including smaller particle size) are more active than for larger particles.

The reaction was repeated with Duratherm-HTO22 as the solvent instead of toluene (Fig. 12). As was seen for the 5 wt% catalysts, the conversions are generally lower in Duratherm than in toluene. Only the $Au/Al_2O_3$ catalyst has a significantly higher conversion in Duratherm than in toluene. This was the case for the 5 wt% catalysts, except that there, $Pt/Al_2O_3$ also performed better in toluene, whereas here it performed slightly worse. The activity trend for carbon-based catalysts is Pt > Pd > Rh ≈ Au, whereas it was Pt > Au > Pd > Rh at 5% loading. For the alumina-supported catalysts, the Pt and Au catalysts are once again the only highly performing catalysts with conversions above 80%, compared with $Rh/Al_2O_3$ and $Pd/Al_2O_3$, which both had conversions around 2%.

Once again, it is surprising that the conversions for these catalysts are generally relatively high despite having 10 times less metal present in the reaction. This may speak to the higher activity of metal particles formed at low loading or that activity is generally very high, and conversion is limited more by other factors, such as diffusion limitations. Overall, combining the catalytic information and the XRD, XPS, and TPR results, it appears that there is a correlation between strongly metallic metal phases and high activity. The more oxidized the metal becomes, the less active it is. Whilst on carbon the metals are mostly metallic, on alumina, there is an increased degree of oxidized phases to a greater or lesser extent depending on the metal. The metals for which the oxidized phase dominates are generally the least active, whereas those that are mostly or entirely metallic are the most active. Notwithstanding that on alumina catalysts seem more likely to become oxidized and therefore inactive, the most active catalysts are also those supported on alumina, albeit in an unoxidized form. It seems that alumina is beneficial to activity as long as the metal oxidation can be prevented.

## Conclusions

The performance of the catalysts tested for the back conversion of QC to NBD in the context of MOST energy storage depends strongly on the choice of metal and support, and the conditions of the measurements, particularly concentration. The catalysts supported on activated carbon are all generally active with moderate to high conversion, depending on the metal. The order of activity for the metals varies depending on the solvent used and the loading, although in all cases, Pt is the most active. On alumina, the activity is strongly dependent on the metal. In all cases, Pt and Au catalysts supported on alumina are active, often strongly active, whereas the Rh and Pd catalysts have low activity or are entirely inactive. The relative activities of the Pt and Au catalysts supported on alumina depend on the solvent and the loading; they are generally similar in terms of conversion in paraffin but are more clearly separated in toluene, although the loading affects which is more active. $Pt/Al_2O_3$ (3 wt%) seems to be the sweet spot in terms of loading.

XRD, XPS, and TPR techniques were used to identify which catalysts had metal in a more reduced or oxidized state. On carbon, all of the catalysts were generally in a reduced state. In contrast, on alumina, Rh and Pd catalysts were primarily or entirely oxidized, whereas the Pt and Au catalysts were primarily or entirely reduced. The reduced catalysts were those that were active, whereas the oxidized ones were inactive. Therefore, it is likely that a metallic state is key to activity in these catalysts.

Catalysts with low loading have disproportionately high activity. The results for the 0.1 wt% catalysts are broadly similar to, though slightly lower than, the results of the 5 wt% catalysts. The 0.1 wt% catalysts were tested with 5 times as much catalyst present in the reaction, but since the loading is 50 times lower, there was only one-tenth the amount of metal present in the reaction. Therefore, the fact that the results are similar to only one-tenth of the metal implies that the metal sites that are present in the 0.1 wt% catalyst are much more active than many of the sites in the 5 wt% catalyst. This may be due to the presence of a small number of easily reduced sites present in both catalysts that are responsible for most of the activity.

## Data availability

The data supporting this article have been included as part of the ESI.†

## Author contributions

B. Rollins: investigation, methodology, visualisation, writing – original draft. A. Gimenez-Gomez: formal analysis, investigation, methodology, visualisation, writing – original draft. A. Steele: resources, project administration, supervision. H. Hölzel: resources. R. J. Salthouse: resources. K. Moreno: resources. K. Moth-Poulsen: conceptualisation, funding acquisition, project administration, supervision. I. Funes-Ardoiz: supervision, validation, visualisation, writing – review & editing. D. Sampedro: conceptualisation, methodology, project administration, supervision, validation.

## Conflicts of interest

There are no conflicts to declare.

## Acknowledgements

This project has received funding from the European Union's Horizon 2020 research and innovation programme under grant agreement No 951801. The authors would like to acknowledge Jason Raymond, Lia JaKyung Murfin, Mark S'ari, Edward Bilbé and Riho T. S. Green from the Advanced Characterization Department at the Johnson Matthey Technology Centre. A. G. G., D. S. and I. F.-A. acknowledge also the projects PID2021-126075NB-I00 and TED2021-131896B-I00 financed by MCIN/AEI/10.13039/501100011033 and the European Union "Next Generation EU"/PRTR. I. F.-A. thanks the MICINN of Spain for financial support (RYC2022-035776-I). K. M.-P. thanks the Catalan Institution for Research & Advanced Studies, ICREA for financial support.

## References

1 A. Behzadi, S. Holmberg, C. Duwig, F. Haghighat, R. Ooka and S. Sadrizadeh, *Renewable Sustainable Energy Rev.*, 2022, **166**, 112625.
2 J. Xu, R. Z. Wang and Y. Li, *Sol. Energy*, 2014, **103**, 610–638.
3 K. E. N'Tsoukpoe and F. Kuznik, *Renewable Sustainable Energy Rev.*, 2011, **139**, 110683.
4 M. Martín, *Comput. Chem. Eng.*, 2022, **165**, 107926.
5 K. Thinsurat, Z. Ma, A. P. Roskilly and H. Bao, *Energy Convers. Manage.: X*, 2022, **15**, 100248.
6 A. Sharma, R. Pitchumani and R. Chauhan, *J. Energy Storage*, 2022, **48**, 104013.
7 A. M. Nair, C. Wilson, M. J. Huang, P. Griffiths and N. Hewitt, *J. Energy Storage*, 2022, **54**, 105227.
8 B. Greening and A. Azapagic, *Renewable Energy*, 2014, **63**, 23–36.
9 A. Giménez-Gómez, L. Magson, C. Merino-Robledillo, S. Hernáez-Troya, N. Sanosa, D. Sampedro and I. Funes-Ardoiz, *React. Chem. Eng.*, 2024, **9**, 1629–1640.
10 A. Lennartson, A. Roffey and K. Moth-Poulsen, *Tetrahedron Lett.*, 2015, **56**, 1457–1465.
11 Z. Wang, P. Erhart, T. Li, Z. Zhang, D. Sampedro, Z. Hu, H. A. Wegner, O. Brummel, J. Libuda, M. B. Nielsen and K. Moth-Poulsen, *Joule*, 2021, **5**, 3116–3136.
12 K. Murayama, H. Tamiaki and S. Kawabata, *J. Chem. Soc., Perkin Trans. 1*, 1986, **1**, 543–549.
13 Z. Wang, Z. Wu, Z. Hu, J. Orrego-Hernández, E. Mu, Z. Zhang, M. Jevric, Y. Liu, X. Fu, F. Wang, T. Li and K. Moth-Poulsen, *Cell Rep. Phys. Sci.*, 2022, **3**, 100789.
14 A. Dreos, K. Börjesson, Z. Wang, A. Roffey, Z. Norwood, D. Kushnir and K. Moth-Poulsen, *Energy Environ. Sci.*, 2017, **10**(728), 2017.
15 V. Kashyap, S. Sakunkaewkasem, P. Jafari, M. Nazari, S. Eslami, S. Nazifi, P. Irajizad, M. D. Marquez, T. R. Lee and H. Ghasemi, *Joule*, 2019, **3**, 3100–3111.
16 C. Schuschke, C. Hohner, M. Jevric, A. U. Petersen, Z. Wang, M. Schwarz, M. Kettner, F. Waidhas, L. Fromm, C. J. Sumby, A. Görling, O. Brummel, K. Moth-Poulsen and J. Libuda, *Nat. Commun.*, 2019, **10**, 2384.
17 A. Dreos, Z. Wang, B. E. Tebikachew, K. Moth-Poulsen and J. Andréasson, *J. Phys. Chem. Lett.*, 2018, **9**, 6174–6178.
18 M. J. Kuisma, A. M. Lundin, K. Moth-Poulsen, P. Hyldgaard and P. Erhart, *J. Phys. Chem. C*, 2016, **120**, 3635–3645.
19 M. Mansø, A. U. Petersen, K. Moth-Poulsen and M. B. Nielsen, *Org. Biomol. Chem.*, 2020, **18**, 2113.
20 J. Zou, B. Zhu, L. Wang, X. Zhang and Z. Mi, *J. Mol. Catal. A: Chem.*, 2008, **286**, 63–69.
21 Z. Wang, A. Roffey, R. Losantos, A. Lennartson, M. Jevric, A. U. Petersen, M. Quant, A. Dreos, X. Wen, D. Sampedro, K. Börjesson and K. Moth-Poulsen, *Energy Environ. Sci.*, 2019, **12**, 187.
22 K. Maruyama and H. Tamaiki, *J. Org. Chem.*, 1986, **51**, 602–606.
23 M. Kajitani, T. Fujita, T. Okumachi, M. Yokoyama, H. Hatano, H. Ushijima, T. Akiyama and A. Sugimori, *J. Mol. Catal.*, 1992, **77**, 1–5.
24 A. L. Tchougréeff, A. M. Tokmachev and R. Dronskowski, *Int. J. Quantum Chem.*, 2013, **113**, 1833–1846.
25 M. E. Landis, D. Gremaud and T. B. Patrick, *Tetrahedron Lett.*, 1982, **23**, 375–378.
26 S. Miki, T. Ohno, H. Iwasaki, Y. Maeda and Z. Yoshida, *Tetrahedron*, 1988, **44**, 55–60.
27 U. Bauer, S. Mohr, T. Döpper, P. Bachmann, F. Späth, F. Düll, M. Schwarz, O. Brummel, L. Fromm, U. Pinkert, A. Görling, A. Hirsch, J. Bachmann, H. Steinrück, J. Libuda and C. Papp, *Chem. – Eur. J.*, 2017, **23**, 1613–1622.
28 U. Bauer, L. Fromm, C. Weiß, P. Bachmann, F. Späth, F. Düll, J. Steinhauer, W. Hieringer, A. Görling, A. Hirsch, H. P. Steinrück and C. Papp, *J. Phys. Chem. C*, 2019, **123**, 7654–7664.
29 R. Eschenbacher, T. Xu, E. Franz, R. Löw, T. Moje, L. Fromm, A. Görling, O. Brummel, R. Herges and J. Libuda, *Nano Energy*, 2022, **95**, 107007.
30 A. Gimenez-Gomez, B. Rollins, A. Steele, H. Hölzel, N. Baggi, K. Moth-Poulsen, I. Funes-Ardoiz and D. Sampedro, *Chem. – Eur. J.*, 2024, **30**, e202303230.
31 C. Li, C. Zhang, R. Liu, L. Wang, X. Zhang and G. Li, *Mol. Catal.*, 2022, **520**, 112170.
32 C. Prado-Burguete, A. Linares-Solano, F. Rodrígues-Reinoso and C. Salinas-Matrínez De Lecea, *J. Catal.*, 1989, **115**, 98–106.
33 A. E. Aksoylu, M. Madalena, A. Freitas, M. Fernando, R. Pereira and J. L. Figueiredo, *Carbon*, 2001, **39**, 175–185.